

Electric-induced reversal of morphogenesis in *Hydra*

Erez Braun^{1,*} and Hillel Ori²

¹Department of Physics, ²Faculty of Medicine,
Technion-Israel Institute of Technology, Haifa 32000, Israel.

*To whom correspondence may be addressed. Email: erez@physics.technion.ac.il

ABSTRACT

Morphogenesis involves the dynamic integration of biochemical, mechanical and electrical processes. We show that an external electric field can halt morphogenesis in *Hydra*. Moreover, above a critical field morphogenesis exhibits reversal dynamics: a fully developed animal folds back into its incipient spheroid morphology. The potential to renew morphogenesis is re-exposed when the field is reduced back to amplitudes below criticality. These dynamics are accompanied by modulations of the *Wnt3* activity, a central component of the head organizer in *Hydra*. Reversal of morphogenesis is shown to be triggered by enhanced electrical excitations in the *Hydra* tissue, leading to intensified calcium activity. The controlled backward-forward cycle of morphogenesis can be repeated several times. These results indicate that electrical processes are tightly integrated with biochemical and mechanical processes in morphogenesis, and play an instructive role to a level that can direct developmental trajectories. The capability to reverse the dynamics of morphogenesis calls for extending the study of development beyond forward-driven hierarchical processes.

Introduction

The capability of animals to generate their entire body-plan from parts is of great interest. How organs and tissues develop in concert to form a functional organism is still largely an open question. Morphogenesis results from the dynamic interplay of three types of processes: biochemical (1-3), mechanical (2, 4) and electrical (5, 6), which span all scales from the molecular to the entire organism (7, 8). While there has been a great progress in understanding the role of each of these processes in morphogenesis, how they are coordinated and integrated towards a robust functional animal remains elusive. Morphogenesis during development has been shown to involve endogenous electrical processes and be sensitive to perturbations affecting transmembrane voltages (6, 9). However, much less is known about the dynamic interactions of the electrical processes with the biochemical and mechanical ones (10).

To investigate the role of electrical processes in morphogenesis we employ external electrical stimulations. *Hydra*, a freshwater animal exhibiting remarkable regeneration capabilities (11), is an interesting model system for that purpose due to the excitable nature of its epithelial tissues which are capable of generating and propagating electrical action potentials (12-14). A tissue segment first goes through an essential stage in which it forms a hollow spheroid made of a bilayer of epithelial cells which eventually regenerates into the body of a mature *Hydra* (15-17). We place small *Hydra* tissue spheroids between a pair of platinum mesh electrodes and study the regeneration dynamics under applied electric fields. We show that there exists a critical electric field which halts the process of regeneration. Remarkably, above this critical field, a fully-developed animal undergoes a reversal trajectory in morphogenesis which is manifested in folding back of its body-plan morphology, simultaneously with the decay of its head organizer signaling activity. The folded tissue maintains its regeneration capability and develops again into a mature animal once the amplitude of the external field is reduced below the critical value. Thus, an external electrical stimulation is used to control the trajectory of morphogenesis without destroying the capability of the tissue to re-develop into a fully mature animal. This cycle of backward-forward trajectory can be repeated a few times without loss of the regeneration potential. Interestingly, the newly emerged body plan in the re-developed folded tissue, is not necessarily similar to the one before the reversal process.

An external electric field is a global physical perturbation capable of stimulating multiple processes in the developing tissue. We find that above a critical amplitude, the external stimulation greatly enhances the electrical excitations in the tissue, which in turn lead to intensified calcium activity in the epithelium. This observation indicates that internal electrical processes trigger the reversal trajectory of morphogenesis. Folding back of the body-plan of a fully developed animal, simultaneously with the decay of a central signaling system at the head organizer, is highly non-trivial. It requires tight integration of the tissue electrical processes, stimulating the reversal dynamics, with mechanical (tissue folding and actomyosin internal force generation) and biochemical (bio-signaling) processes, in order to keep the integrity of the backward folded tissue. Moreover, it shows that there is no privilege process (e.g., biochemical) or level of organization in determining developmental trajectories; in our case, under the external stimulation, the electrical processes can direct morphogenesis.

Results

In the absence of external electric fields, *Hydra* regenerate from incipient tissue spheroids into mature animals within 15–55 hrs (16). The regeneration trajectory is significantly affected by an applied voltage (Fig. 1). The application of an AC electric field with a critical voltage amplitude of ~20–30 Volts at 1 kHz frequency, halts regeneration and the tissue does not develop (Figs. 1a,b; Fig. S1). The suspended tissue maintains its regeneration potential as proved by the resumption of morphogenesis upon the reduction of the external voltage below the critical value (Fig. 1b; Fig. S1). When the voltage is increased above the critical value after the regeneration process concluded, a fully developed *Hydra* gradually shrinks its tentacles and eventually folds back its mature body-plan into the incipient morphology of a spheroid (Fig. 1c; Fig. S2). The reversal of morphogenesis is gradual and can be controlled to some extent by the external voltage. However, different tissues exhibit different critical voltages. The practical difficulty in precisely controlling the morphogenesis trajectory is due to the individual sensitivity of each tissue to the applied voltage and the fact that above the critical value, which cannot be *a-priori* determined, too high external potential can lead to irreversible disintegration of the tissue and loss of its regeneration capability. However, if the voltage increase is gradual and carefully controlled near the critical value, the tissue maintains its integrity as well as its regeneration capacity for repeated cycles of backward-forward morphogenesis (Supplementary Movie 1). This remarkable reversal of morphogenesis is reproducible and robust as summarized in the cumulative distributions of 15 experiments in Fig. 1d. It shows that below the critical voltage (blue curve, left) regeneration (defined by the emergence of tentacles) emerges for all samples (147) in less than ~55 hrs. At voltages above criticality, however, the probability to observe tentacles in the back-folding samples diminishes within a wide range of time scales, and is practically zero above ~90 hrs. All 77 samples in Fig. 1d (red curve, right) first regenerate into mature animals and then fold back upon the increase of the external voltage.

Renewed morphogenesis upon the reduction of the applied voltage, does not necessarily lead to the same morphology as in the previous cycle, e.g., manifested by a different number of tentacles or their shape (Fig. S2). The cycle of controlled backward-forward morphogenesis can be repeated a few times. The second cycle of backward folding requires higher voltage to reverse

morphogenesis than the first one (see examples in Fig. 4a; Fig. S2). This increase in the critical voltage points to an interesting adaptation of the tissue.

We next examine whether reversal morphogenesis has a signature in the underlying biological processes beyond the observed change in morphology. We utilize a transgenic *Hydra* expressing a GFP probe under the control of the *Wnt3* promoter (18, 19). *Wnt3* is a component of the canonical *Wnt* pathway, which has been shown to be key in patterning the body plan in many organisms and in *Hydra* is an essential component of the head organizer (18, 20). The *Hydra* head organizer is a well-defined group of cells in which *Wnt3* is maintained continuously active by an autoregulatory transcriptional system (18) and plays an important role in preserving the integrity of the body-plan in face of continuous replacement of tissues in a developmental process that never ceases (21). The *Wnt3* signal is thus a relevant marker for the underlying biological state of the tissue in morphogenesis. Remarkably, the *Wnt3*-activity fluorescence signal that emerges at the tip of the head (hypostome) in mature *Hydra* (18, 20), gradually decays after the external voltage is increased beyond criticality, marking the decay of the head organizer activity as the tissue folds back into an incipient spheroid (Fig. 2). The *Wnt3* signal re-emerges upon a second round of regeneration, following switching of the external voltage to zero (Supplementary Movie 2). Overall, we examined 18 samples of fully regenerated *Hydra*, reversing its morphology together with the decay of the *Wnt3*-activity fluorescence signal (examples in Fig. S3).

To gain insight into the mechanism of reversible morphogenesis, we next study the effect of the external field on calcium dynamics. Calcium is an important universal effector across systems and an important mediator between mechanical, electrical and biochemical processes (10). Towards this end, we constructed a transgenic *Hydra* expressing a fast Ca^{2+} fluorescence probe (22) in its epithelial cells (Methods). Tissue fragments excised from these transgenic *Hydra* are placed in the experimental setup after folding into spheroids and time-lapse movies at 1 min resolution are recorded. In the absence of external electric fields, the tissue initially exhibits local excitations of the Ca^{2+} signals at different parts, which eventually become coordinated into sporadic whole-tissue coherent spikes (Figs. 3a,b). Elevated external voltage (>15 V, 1 kHz), leads to a significant increase in the Ca^{2+} activity manifested in an increased density of the Ca^{2+} spikes train riding on an enhanced baseline. Even more enhanced activity is observed above a

critical voltage of ~ 20 V (Fig. 3a, arrow at the lower trace), with prolonged periods showing almost continuous enhanced activity.

Applying an external voltage immediately following the folding of the excised tissue to a spheroid, Fig. 3c (upper trace; Fig. S4a) depicts the fluorescence density of the initial spheroid tissue under 15 V (1 kHz). At this voltage, which is somewhat below the critical value, the tissue immediately exhibits a significant level of Ca^{2+} activity, which apparently is not enough to halt morphogenesis (see attached images, Fig. 3d; Fig. S4a). Increasing the voltage above criticality however, increases the level of Ca^{2+} activity (Fig. 3c, middle trace; Fig. S4b) causing in turn the folding of the already patterned *Hydra* back into the incipient spheroid (upper image in Fig. 3e; Fig. S4b). Finally, switching the voltage to zero reduces Ca^{2+} activity (Fig. 3c, bottom trace; Fig. S4c) and leads to the recovery of morphogenesis and renewed regeneration of a mature *Hydra* (lower image in Fig. 3e; Fig. S4c), indicating that the tissue maintains its regeneration potential (Supplementary Movie 3). The normalized distributions of fluorescence densities in Fig. 3f quantify the Ca^{2+} activity, showing enhanced tails at elevated external voltages (red) compared to zero voltage (blue).

We next show that the elevated Ca^{2+} activity leading to reversal of morphogenesis is a manifestation of enhanced electrical excitability. This is demonstrated along three different experimental lines. First, we demonstrate the existence of a frequency cutoff for the AC electric field, above which the tissue becomes insensitive to the applied field; morphogenesis proceeds normally and no reversal is observed. Fig. 4a shows Ca^{2+} traces at two different frequencies of the external field. The initial tissue spheroid first regenerates into a mature *Hydra* at $V=0$, showing a typical low level of Ca^{2+} activity (Fig. 4a, first trace; Fig. S5a). Increasing the external voltage above the critical value (26.5 V) at 1 kHz, leads to a significant elevation in the level of Ca^{2+} activity and folding of the mature *Hydra* back into a spheroid morphology (Fig. 4a, second trace; Fig. S5b). Increasing the AC frequency to 3 kHz while maintaining the same amplitude, results in reduced Ca^{2+} activity and re-emergence of a regenerated mature *Hydra* (Fig. 4a, third trace; Fig. S5c). The frequency sensitivity is summarized in Fig. 4b, showing the normalized distributions of fluorescence density at zero and high voltage at 1 kHz (20-26.5 V) and 3 kHz (26.5 V). The Ca^{2+} activity at 3 kHz is very comparable to that at zero voltage, while the activity

at 1 kHz is significantly enhanced. Repeating this frequency-switching cycle, Fig. 4a (fourth trace) shows the re-emergence of an elevated Ca^{2+} activity and backwards folding of morphogenesis into a spheroid upon switching back to 1 kHz. This second cycle of backward folding however, requires higher critical voltage to reverse morphogenesis than the first one ($V > 30$ V). Finally, switching frequency again to 3 kHz reduces Ca^{2+} activity and leads to the emergence of a re-regenerated mature *Hydra* (Fig. 4a, bottom trace). These data demonstrate the existence of a frequency cutoff around 1 kHz, above which the elevated Ca^{2+} activity is reduced and morphogenesis is restored from its suspended state. Further experiments demonstrate that at frequencies higher than 1 kHz, the regeneration process is insensitive to the external electric field (Supplementary Movie 4). The ~ 1 kHz frequency threshold, above which the tissue becomes “transparent” to the applied external voltage, strongly suggests a corresponding characteristics timescale of the order of a few milliseconds, which is consistent with the measured capacitance (RC) time constant of the *Hydra* tissue (23).

Second, we follow the tissue dynamics under an elevated external potassium (K^+) concentration which serves as a standard method to stimulate excitable tissues, as demonstrated also in *Hydra* (24). Fig. 4c shows that increasing potassium concentration in the medium from 0.1 mM (normal medium; upper trace) to 1 mM (lower trace), indeed leads to elevated Ca^{2+} activity (see also the normalized distributions in Fig. 4d). Importantly, this is accompanied by folding back of the regenerated *Hydra*. The tissue seems to lose its regeneration capability following the high potassium treatment. Nevertheless, it is clear that elevated potassium excites the system and leads to reversal morphogenesis similar to that observed under an external electric field (Fig. S6).

Finally, we directly measure the time-dependent electrical potential by inserting a silver-chloride electrode into a tissue segment embedded in a low-melting 2% agarose gel that damps its motion, while simultaneously recording fluorescence images of the Ca^{2+} signal under the microscope. Fig. 4e shows that every Ca^{2+} spike is stimulated by a pre-burst of action potentials (13, 25) (167/174 measured Ca^{2+} spikes show clear pre-bursts of action potentials leading them; see also Fig. S7).

These three pieces of evidence: frequency threshold, excitations due to elevated potassium and direct electrical recordings, point to enhanced electrical activity of the *Hydra* tissue as the source

of elevated Ca^{2+} activity and thus to the mechanism triggering reversal morphogenesis. Previous works indeed showed that external electric fields, within the same range used in our experiments, cause enhanced electrical activity, leading for example to enhanced discharge of nematocytes (24).

Discussion

While the mechanism leading from enhanced Ca^{2+} activity to reversal of morphogenesis requires further research, the observed phenomenon whereby this reversal process is driven by electrical excitations has already at this stage some important implications. First, morphogenesis is usually considered a hierarchical forward-driven process, in which each stage switches-on the next one till the completion of a body plan (26). It was shown before that under metabolic stress *Hydra* can lose its tentacles and change its body morphology in a reversible way, but this phenomenon was not further investigated (27). The observation that an external physical manipulation in the form of an electric field, by triggering enhanced electrical excitations of the tissue, can halt morphogenesis and even reverse it in a controlled way without destroying the regeneration potential of the tissue, paints a picture of morphogenesis in which electrical processes play an instructive role to a level that can direct developmental trajectories not obeying this hierarchy (5). Second, it shows that the electrical processes are tightly integrated with the underlying mechanical (e.g., tissue folding) (10) and biochemical (e.g., *Wnt3* expression) ones. In particular, the decay of the head organizer during reversal of morphogenesis demonstrates that the changes in the tissue encompass more than mere morphology, and also involve significant rearrangements in the underlying biological processes. How deep these biological transformations are, e.g. in reprogramming differentiated cells into stem cells, remains an exciting question for future studies. The ability to stimulate reversal of morphogenesis by an external electric field opens up new ways to further study the symbiotic dynamics of these different processes in morphogenesis. In particular, the ability to halt morphogenesis at different time points and reverse its dynamic trajectory enables us to identify the types of information stored in the developing tissues, the reservoirs of ions and biomolecules and structural memories (16) instilled in the tissue and playing a role in the regeneration process. Furthermore, the ability

to block regeneration in a controllable fashion can shed light on the origin of a tissue's regeneration potential and reveal the reasons some tissues can readily regenerate while others cannot do so.

Third, controlled reversal morphogenesis opens the possibility for a new approach in the study of developmental systems (28, 29): One would like to study the potential of a given system to realize different developmental trajectories, beyond the canalized one (10). Currently, this can be done only by studying an ensemble of different systems. Halting, reversing and re-initiating a developmental process of a given system at different time points, open up a possibility for studying the developmental potential rather than an instantiation of it.

Figures:

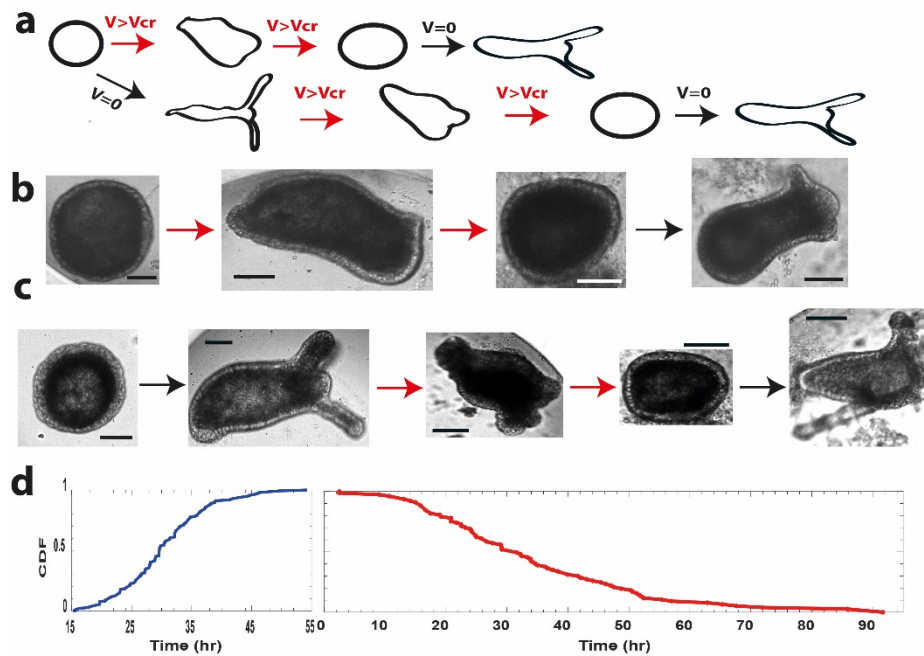


Fig. 1: Halt and reversal of morphogenesis under an external electric field. (a) Possible trajectories for an incipient spheroid tissue under a field. (b) Images depicting the trajectory scheme in (a) top row: Time (hrs from tissue excising) and voltages (Volts) for the images (from left): 5.5, 0; 42, 18; 68, 25.5; 97, 0. The voltage is switched off at 71 hrs. Bars 100 μ m scale. (c) Images depicting the trajectory scheme in (a) bottom row: Time (hrs from tissue excising) and voltages (Volts) for the images (from left): 2, 0; 53, 0; 80, 25; 108, 31; 136, 0. The voltage is switched off at 108 hrs. Bars 100 μ m scale. (d) Cumulative statistics for regeneration and reversal of morphogenesis. (left) Cumulative statistics for 147 samples exhibiting their first regeneration in the absence of an external voltage or a voltage below the critical value. Time is measured from the point of tissue excision and regeneration is identified as the emergence of tentacles. All samples regenerated between 15-55 hrs, in agreement with previous results (16). (right) Cumulative statistics for reversal of morphogenesis, the folding back of fully regenerated *Hydra* into the incipient spheroid morphology, for 77 samples. All samples first regenerated into a mature *Hydra*. Folding time is estimated from the point at which the voltage was first set above 15 V, the minimal voltage observed to affect morphology (e.g., shortening of the tentacles).

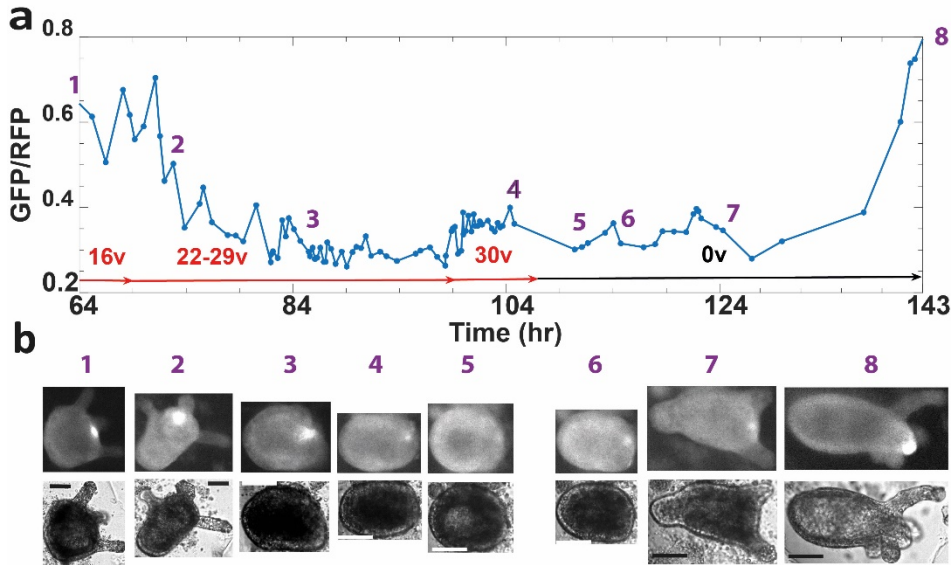


Fig. 2: The decay of *Wnt3* activity upon reversal of morphogenesis. Transgenic *Hydra* expressing a GFP probe under the control of the *Wnt3* promoter and dsRED (RFP; serving as a reference, Fig. S3) under the ubiquitous *Hydra* actin promoter (18, 19), imaged at 1 min time-lapse microscopy. (a) The *Wnt3* activity at different time points (from the tissue excision time) is estimated from the average fluorescence ratio of GFP/RFP in a small region around the center of the GFP signal. The tissue first regenerated into a mature *Hydra* in the absence of an external field, expressing a clear GFP signal at the head organizer. An external field above the critical voltage, leads to reversal of morphogenesis and the decay of the *Wnt3* signal (1-5). Resumption of regeneration leading to a mature *Hydra* and the reemergence of the *Wnt3* signal after the voltage is switched off (6-8). The curve measures the trajectory of the *Wnt3*-activity decay, as the voltage is increased (Voltage values marked in red), and its recovery upon the renewal of regeneration. (b) Fluorescence images of the GFP channel (upper row) and the corresponding bright-field images (lower row) at time points marked in (a). Bars 100 μ m scale.

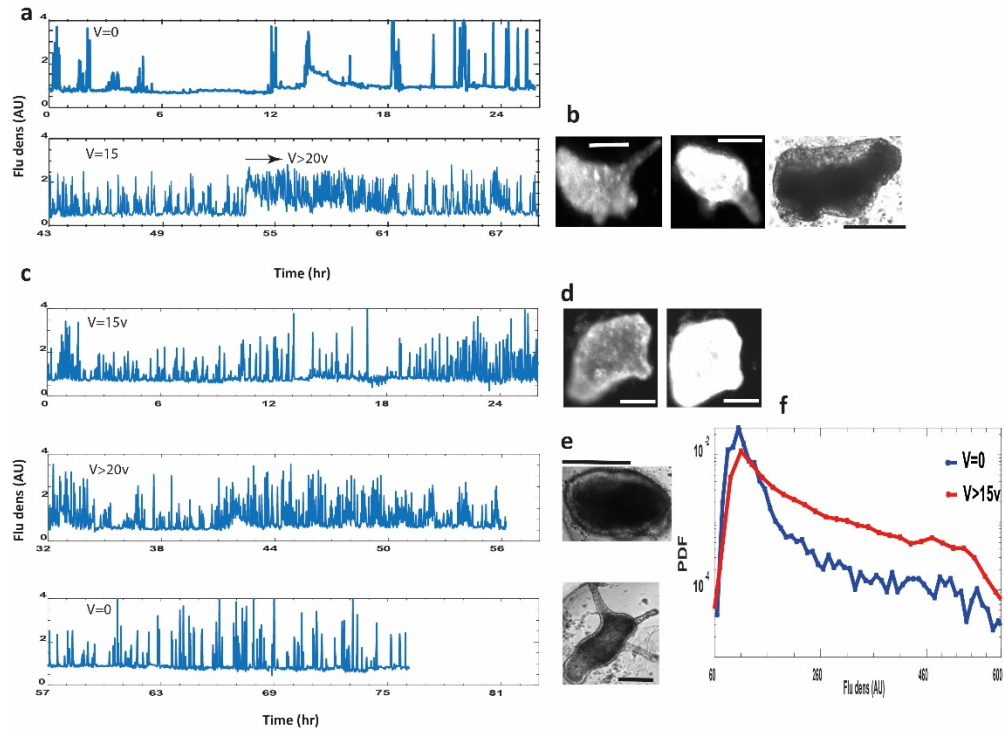


Fig. 3: Calcium dynamics. A transgenic *Hydra* expressing the fast Ca^{2+} fluorescence probe (22) in its epithelial cells is utilized. (a) Ca^{2+} dynamics as measured by the fluorescence density (fluorescence signal per unit area) at $V=0$ (upper trace) and at high external voltage (lower trace). The measurement starts 3 hrs after the tissue excision. The lower trace starts at 15 V, which is below the critical value, and the voltage is then increased to higher values (25 V; arrow). The traces show the fluorescence density divided by the mean over the entire trace. (b) Fluorescence images of the sample (at the end of the trace), at the baseline and high activity (two left images: 69 hrs from excision, 25 V) and a BF image (right; 79 hrs, 25 V). (c) Ca^{2+} activity (as in (a)) of a tissue under 15 V at the onset of the measurement (upper trace). Voltage is increased to 24 V (middle trace) and then switched off (lower trace). (d) Fluorescence images of low and high Ca^{2+} activity at the end of the upper trace (29 hrs, 15 V). Note the tentacles indicating that the tissue regenerated. (e) BF images showing reversal of the morphology at the end of the middle trace, and resumption of regeneration at the end of the lower trace (top image: 63 hrs, 24 V; lower image: 77 hrs, 0 V). (f) Normalized distributions of fluorescence densities at $V=0$ (blue) and high voltage (>15 V; red). Each curve summarizes 9 samples overall with more than 10,000 measurement points. Note the logarithmic scale.

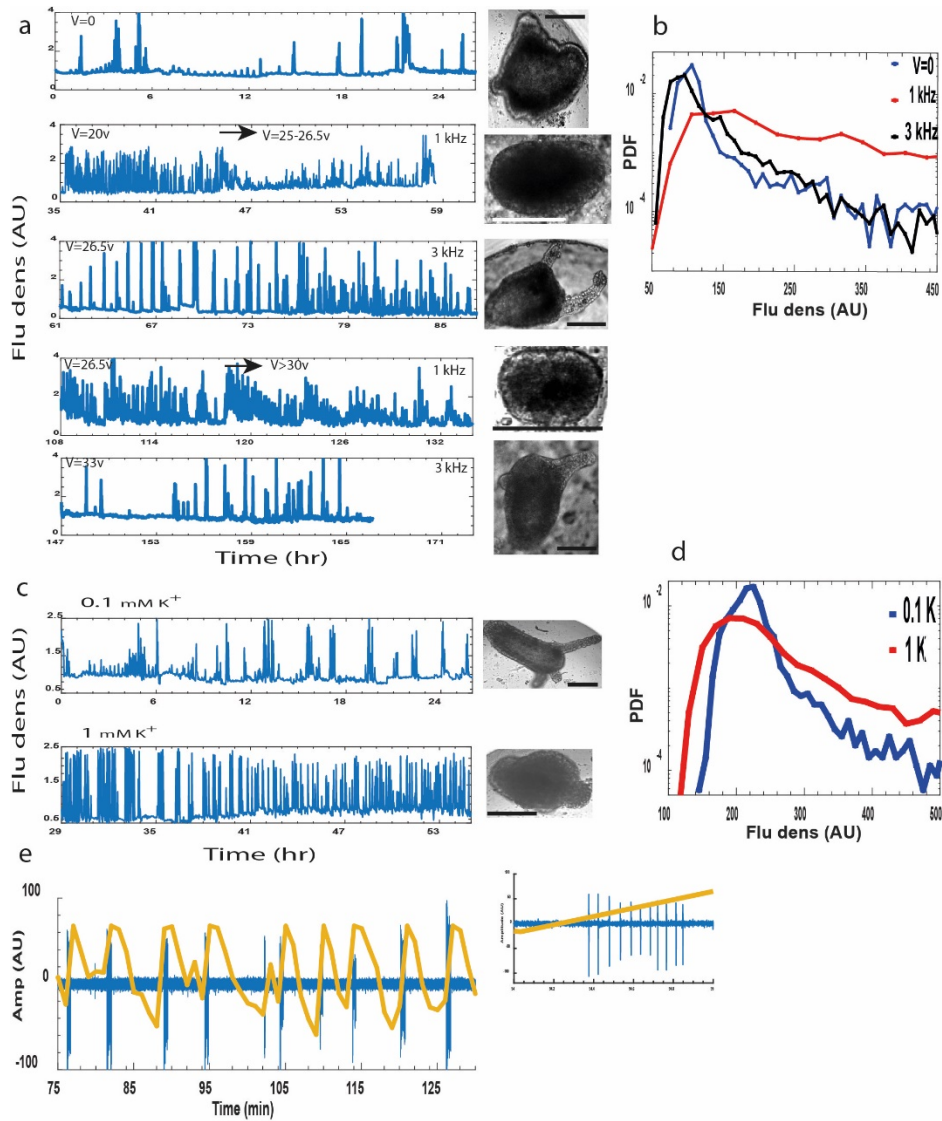


Fig. 4: Enhanced electrical excitability of the tissue triggering reversal of morphogenesis. (a) Ca^{2+} fluorescence density for $V=0$ (first trace) and 20-26.5 V at 1 kHz (second trace). Bf images (at end point of each corresponding trace). (Third trace) 26.5 V, 3 kHz, showing resumption of a fully regenerated *Hydra* (attached image). (b) Normalized fluorescence density distributions comparing: $V=0$ (blue), high voltage at 1 kHz (red) and 3 kHz (black). Each curve summarizes two samples, with 2800-4500 measured points at 1 min resolution. Note the logarithmic scale. Repeated frequency switching; 1 kHz at the same voltage (26.5 V; fourth trace). Increased voltage (33 V), leads to reversal of morphogenesis (attached image). A second frequency switch to 3 kHz (fifth trace). (c) Ca^{2+} fluorescence density for: 0.1 mM (normal medium; upper trace) and 1 mM (lower trace) medium K^+ . Attached Bf images at the end point of the corresponding trace. (d) Fluorescence density distributions for 1 mM (red) and 0.1 mM (blue) K^+ . Note the logarithmic scale. (e) Direct measurement of the electrical potential by a silver-chloride electrode. Each Ca^{2+} spike (yellow) is stimulated by a pre-burst of action potentials (blue; Methods). Inset: a zoom over one of the Ca^{2+} spike events. Overall we measured 107 Ca^{2+} spikes in tissue fragments with only 5 among them with no clear burst of electrical spikes (see Fig. S7b for a measurement of a spheroid tissue).

References:

1. J. B. A. Green, J. Sharpe, Positional information and reaction-diffusion: two big ideas in developmental biology combine. *Development* **142**, 1203-1211 (2015).
2. C. J. Miller, L. A. Davidson, The interplay between cell signalling and mechanics in developmental processes. *Nature Rev. Genetics* **14**, 733-744 (2013).
3. P. A. Lawrence, Morphogens: how big is the big picture? *Nature Cell Biology* **3**, E151-E154 (2001).
4. T. Mammoto, A. Mammoto, D. E. Ingber, Mechanobiology and Developmental Control. *Annual Review of Cell and Developmental Biology* **29**, 27-61 (2013).
5. M. Levin, C. J. Martyniuk, The bioelectric code: An ancient computational medium for dynamic control of growth and form. *Biosystems* **164**, 76-93 (2018).
6. M. Levin, G. Pezzulo, J. M. Finkelstein, Endogenous bioelectric signaling networks: Exploiting voltage gradients for control of growth and form. *Annual Review of Biomedical Engineering* **19**, 353-387 (2017).
7. G. B. Müller, S. A. Newman, in *Vienna Series in Theoretical Biology*. (MIT Press, Cambridge, 2003).
8. K. D. Atabay, S. A. LoCascio, T. de Hoog, P. W. Reddien, Self-organization and progenitor targeting generate stable patterns in planarian regeneration. *Science* **360**, 404-409 (2018).
9. K. A. McLaughlin, M. Levin, Bioelectric signaling in regeneration: Mechanisms of ionic controls of growth and form. *Developmental biology* **433**, 177-189 (2018).
10. E. Braun, K. Keren, Hydra Regeneration: Closing the Loop with Mechanical Processes in Morphogenesis. *BioEssays* **40**, 1700204 (2018).
11. A. Gierer *et al.*, Regeneration of hydra from reaggregated cells. *Nature/New Biology*, 98-101 (1972).
12. R. D. Campbell, R. K. Josephson, W. E. Schwab, N. B. Rushforth, Excitability of nerve-free hydra. *Nature* **262**, 388-390 (1976).
13. R. K. Josephson, M. Macklin, Transepithelial Potentials in Hydra. *Science* **156**, 1629-1631 (1967).
14. G. Kass-Simon, V. K. Diesl, Spontaneous and evoked potentials from dissociated epithelial cells of Hydra. *Nature* **265**, 75-77 (1977).
15. C. Fütterer, C. Colombo, F. Julicher, A. Ott, Morphogenetic oscillations during symmetry breaking of regenerating Hydra vulgaris cells. *EPL* **64**, 137 (2003).
16. A. Livshits, L. Shani-Zerbib, Y. Maroudas-Sacks, E. Braun, K. Keren, Structural inheritance of the actin cytoskeletal organization determines the body axis in regenerating hydra. *Cell Reports* **18**, 1410-1421 (2017).
17. M. Kucken, J. Soriano, P. A. Pullarkat, A. Ott, E. M. Nicola, An osmoregulatory basis for shape oscillations in regenerating Hydra. *Biophys J* **95**, 978-985 (2008).
18. Y. Nakamura, C. D. Tsiairis, S. Ozbek, T. W. Holstein, Autoregulatory and repressive inputs localize Hydra Wnt3 to the head organizer. *PNAS* **108**, 9137-9142 (2011).
19. M. C. Vogg *et al.*, An evolutionarily-conserved Wnt3/ β -catenin/Sp5 feedback loop restricts head organizer activity in Hydra. *Nature Communications* **10**, 312 (2019).
20. B. Hobmayer *et al.*, WNT signalling molecules act in axis formation in the diploblastic metazoan Hydra. *NATURE* **407**, 186-189 (2000).
21. H. R. Bode, The head organizer in Hydra. *Int. J. Dev. Biol.* **56**, 473-478 (2012).
22. C. Dupre, R. Yuste, Non-overlapping neural networks in Hydra vulgaris. *Current Biology* **27**, 1-13 (2017).

23. R. K. Josephson, M. Macklin, Electrical Properties of the Body Wall of *Hydra*. *The Journal of General Physiology* **53**, 638-665 (1969).
24. A. H. Gitter, D. Oliver, U. Thurm, Calcium- and voltage-dependence of nematocyst discharge in *Hydra vulgaris*. *Journal of Comparative Physiology A* **175**, 115-122 (1994).
25. T. Itayama, Y. Sawada, Development of electrical activity in regenerating aggregates of hydra cells. *Journal of Experimental Zoology* **273**, 519-526 (1995).
26. S. F. Gilbert *Developmental Biology*. (Sinauer Associates, Inc., ed. 10, 2013).
27. S. A. Newman, Reversible Abolition of Normal Morphology in Hydra. *Nature New Biology* **244**, 126 (1973).
28. L. S. Vygotsky, in *Mind in Society; the Development of Higher Psychological Processes* M. Cole, V. John-Steiner, S. Scibner, E. Souberman, Eds. (Harvard University Press, Cambridge Mass, 1978), chap. 5, pp. 58-79.
29. S. Marom, *Science, Psychoanalysis, and the Brain: space for dialogue* (Cambridge University Press, New York, 2015).

Acknowledgements

We thank Kinneret Keren for helpful discussions and comments on the manuscript. We thank Shimon Marom and Naama Brenner for comments on the manuscript. We thank our lab members: Anton Livshits, Lital Shani-Zerbib, Yonit Maroudas-Sacks and Liora Garion for technical help. Special thanks to Gdalyahu Ben-Yoseph for superb technical help in designing and constructing the experimental setup and in providing the infrastructure enabling the experiments.

We thank: Prof. Thomas Bosch and Dr. Alexander Klimovich for their help in generating the Ca^{2+} strain; Prof. Bert Hobmayer for generously providing the transgenic *Hydra* expressing lifeact; Prof. Brigitte Galliot for generously providing the *Wnt3* strain that was first constructed in Prof. Thomas Holstein lab.

Funding: E.B. acknowledged support by the Israel Science Foundation, Grant # 228/17.

Materials and Methods

Hydra strains, culture and sample preparation

Experiments are carried out with three transgenic strains of *Hydra Vulgaris* (AEP): A HyWnt3:GFP-HyAct:dsRED transgenic strain (a generous gift from B. Galliot University of Geneva (19) utilizing the hoTG-HyWnt3FL-EGFP-HyAct:dsRED plasmid from T. Holstein, Heidelberg (18)); A transgenic line with a GCaMP6s probe reporting Ca^{2+} activity we generated in the Kiel center using a modified version of the pHyVec1 plasmid (Addgene catalog no. 34789) which replaces the GFP sequence with a GCaMP6s sequence that was codon-optimized for *Hydra* (22). The embryos were grown and propagated for a few weeks. We selected *Hydra* expressing GCaMP6s in their epithelium cells and propagate them until a stable signal covering the entire animal emerges throughout the population. A third transgenic line expressing lifeact-GFP in the ectoderm (generously provided by Prof. Bert Hobmayer, University of Innsbruck, Austria) (16), is also used in some experiments, allowing to verify the folding-back of the *Hydra* into a spheroid by imaging the actin fibers. The reversal of morphogenesis phenomenon is found to be similar for all strains. Animals are cultivated in *Hydra* culture medium (1mM NaHCO₃, 1mM CaCl₂, 0.1mM MgCl₂, 0.1mM KCl, 1mM Tris-HCl pH 7.7) at 18°C. The animals are fed every other day with live *Artemia nauplii* and washed after ~4 hours. Experiments are initiated ~24 hours after feeding.

Tissue segments are excised from the middle of a mature *Hydra* using a scalpel equipped with a #15 blade. To obtain fragments, a ring is cut into ~4 parts by additional longitudinal cuts. Fragments are incubated in a dish for ~3 hrs to allow their folding into spheroids prior to transferring them into the experimental sample holder. Regeneration is defined as the appearance of tentacles, and the regeneration time is defined as the time interval between excision and the appearance of the first tentacle.

Sample holder

Spheroid tissues are placed within wells of ~1.3 mm radius made in a strip of 2% agarose gel (Sigma) to keep the regenerating *Hydra* in place during time lapse imaging. The tissue spheroid typically of a few hundred μm is free to move within the well. The agarose strip containing 12-13 wells, is fixed on a transparent plexiglass bar of 1 mm height, anchored on a Teflon holder within a 55 mm Petri dish. Two platinum mesh electrodes (Platinum gauze 52 mesh, 0.1 mm dia. Wire; Alfa Aesar) are stretched and fixed by 2% agarose gel from the two sides of the plexiglass bar at a distance of 4 mm, leaving two channels for fluid flow between the electrodes and the samples. The mesh electrodes cover the entire length of the sample holder and their height ensures full coverage of the samples. A peristaltic pump (IPC, Ismatec) flows the medium continuously from an external reservoir (replaced at least once every 24 hrs) at a rate of 170 ml/hr into each of the channels between the electrodes and the samples. The medium

covers the entire preparation and the volume in the bath is kept fixed throughout the experiments by pumping medium out from 3 holes which determine the height of the fluid. The continuous medium flow ensures stable environmental conditions and the fixed volume of medium in the bath ensures constant conductivity between the electrodes. All the experiments are done at room temperature.

AC generators

An alternating current (AC) generator (PM5138A, Fluke; or a waveform generator 33621A, Agilent connected to a voltage amplifier A-303, A.A. Lab Systems for voltages above 40 V) is used to set the voltage between the electrodes. The generator is connected directly to one of the electrodes and via a current multimeter (34401A, HP) to the second one, allowing to monitor the current in the system throughout the experiment. The measured current is around 4 mA for applied 10 V and the conductivity is found to be linear with the increase of applied voltage throughout the experiment. The connection to the platinum electrodes is made by sintering 0.4 mm wide platinum wires (Alfa Aesor) to the mesh electrodes, allowing contacts to the external devices with only Pt in contact with the medium.

Microscopy

Time lapse bright-field and fluorescence images are taken by a Zeiss Axio-observer microscope (Zeiss) with a 5× air objective (NA=0.25) with a 1.6× optovar and acquired on a CCD camera (Zyla 5.5 sCMOS, Andor). The sample holder is placed on a movable stage (Marzhauser) and the entire microscopy system is operated by Micromanager, recording images at 1 min resolution.

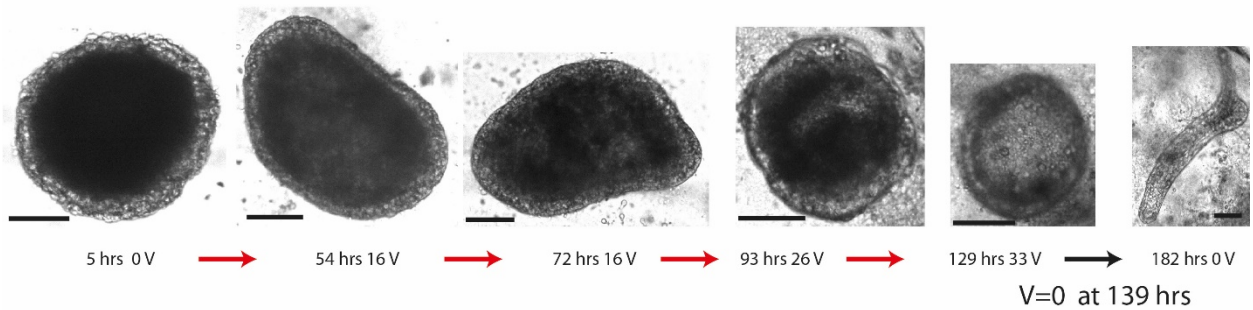
Electrophysiology

Tissue fragments before folding or tissue spheroids after folding, are immersed in 2% low-gelling agarose (Sigma) covered with a standard medium, placed within a 90 mm petri dish. The measurements are done under a fluorescence microscope (Zeiss Observer), allowing simultaneous fluorescence and electrical measurements. Microelectrodes are fabricated by AgCl coated silver wires, threaded in glass capillaries (1.5mm OD and 0.86mm ID, A-M systems). Capillaries are pulled, broken at the extreme tip, and filled with a standard medium solution. A reference electrode made of a thick AgCl coated silver wire is immersed in the dish. The microelectrode is placed on a manipulator and allowed to penetrate the tissue until a stable resting potential is measured. Voltage is measured using AxoPatch 200B amplifier (Axon Instruments) and measurements are inspected by an oscilloscope, as well as digitally acquired at 1000Hz frequency by NI PCI-6259 acquisition card (National Instruments). Time lapse imaging is done at 1 min resolution in bright field and fluorescence channels allowing to image the tissue and record the Ca^{2+} activity.

To extract the recorded spike train, the voltage trace is smoothed (0.1 sec window) and the smoothed trace is subtracted from the original voltage trace. The filtered trace is magnified to emphasize the spikes. The Ca^{2+} activity recorded by the time-lapse fluorescence signal is extracted from each frame within a circle smaller than the tissue fragment to avoid edge effects. The Ca^{2+} signal is manually adjusted to the electrical recording by monitoring the precise starting point of the time-lapse measurement.

Supplementary Figures:

a



b

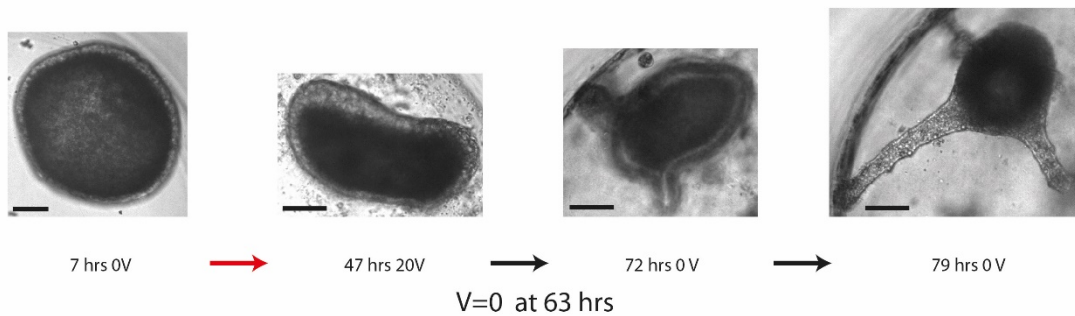


Fig. S1: Examples of halted regeneration by an external electric field. A series of images from two experiments (a, b) depicting the trajectory scheme in Fig. 1a top row of the main text. Time (hrs from tissue excising) and voltages (Volts) are indicated for each image. The tissues do not develop under the electric field above its critical value (specific for each tissue; 1 kHz) until time points extending the maximal regeneration time observed in our experiments (~55 hrs) and they readily regenerate into a mature *Hydra* upon switching the voltage to zero at the indicated time. Bars 100 μ m scale.

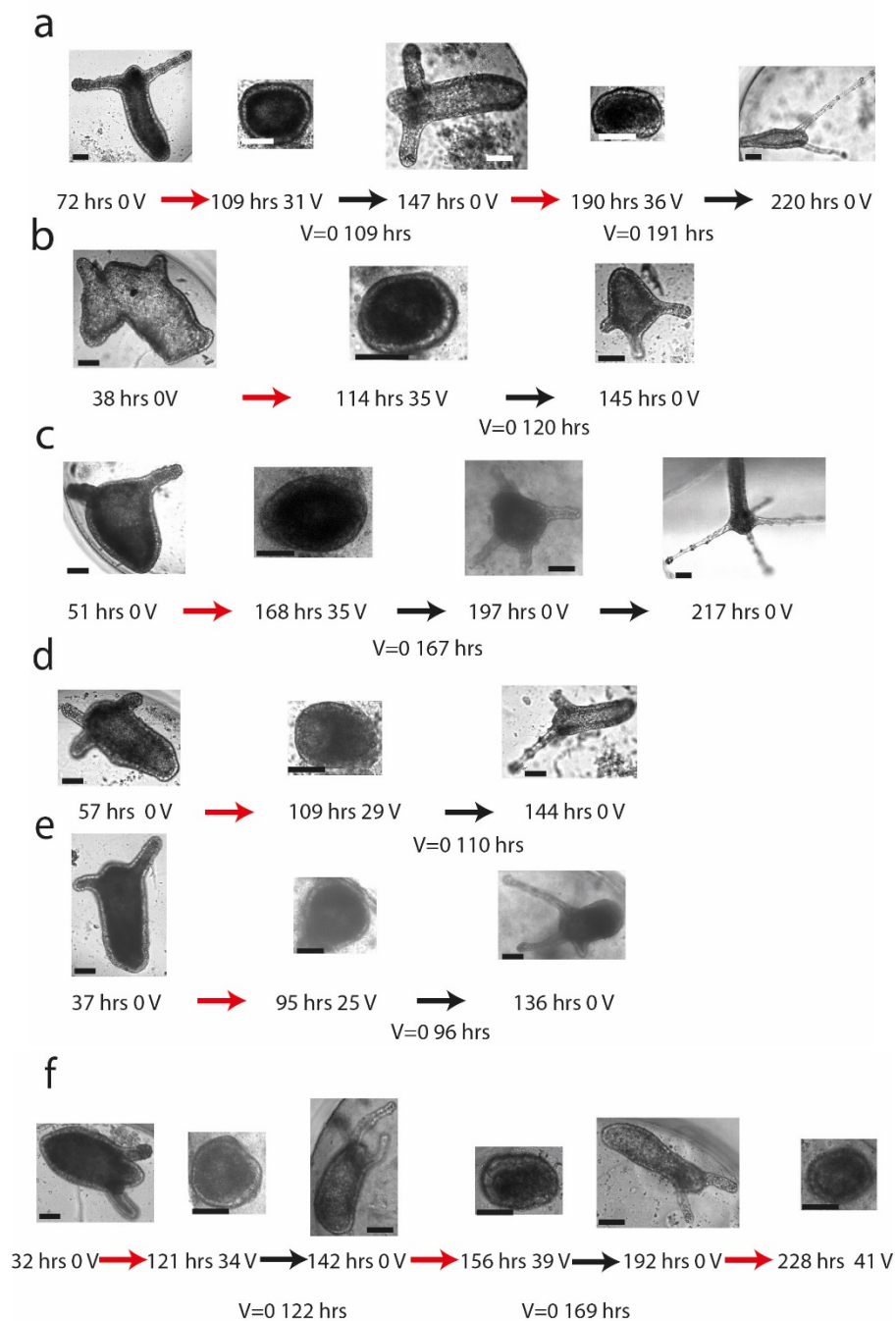


Fig. S2: Examples of reversal of morphogenesis under an external electric field and the emergence of new morphologies upon renewal of regeneration. A series of images depicting the trajectory scheme in Fig. 1a bottom row of the main text. Each row of images (a-f) is a separate experiment. Time (hrs from tissue excising) and voltages (Volts) are depicted below the images (external AC field at 1 kHz). In all the experiments presented here, the spheroid tissue first regenerates into a mature Hydra and then folds back into a spheroid upon the increase of the externally applied voltage above the critical value (specific for each tissue). The reversed tissue regenerates again upon the reduction of the external voltage to zero at the indicated time. Note that the emerged renewal morphology is in some of the cases not similar to the initial morphology. The images in (a,f) demonstrate that this backward-forward cycle of morphogenesis can be repeated for the same tissue. Bars 100 μ m scale.

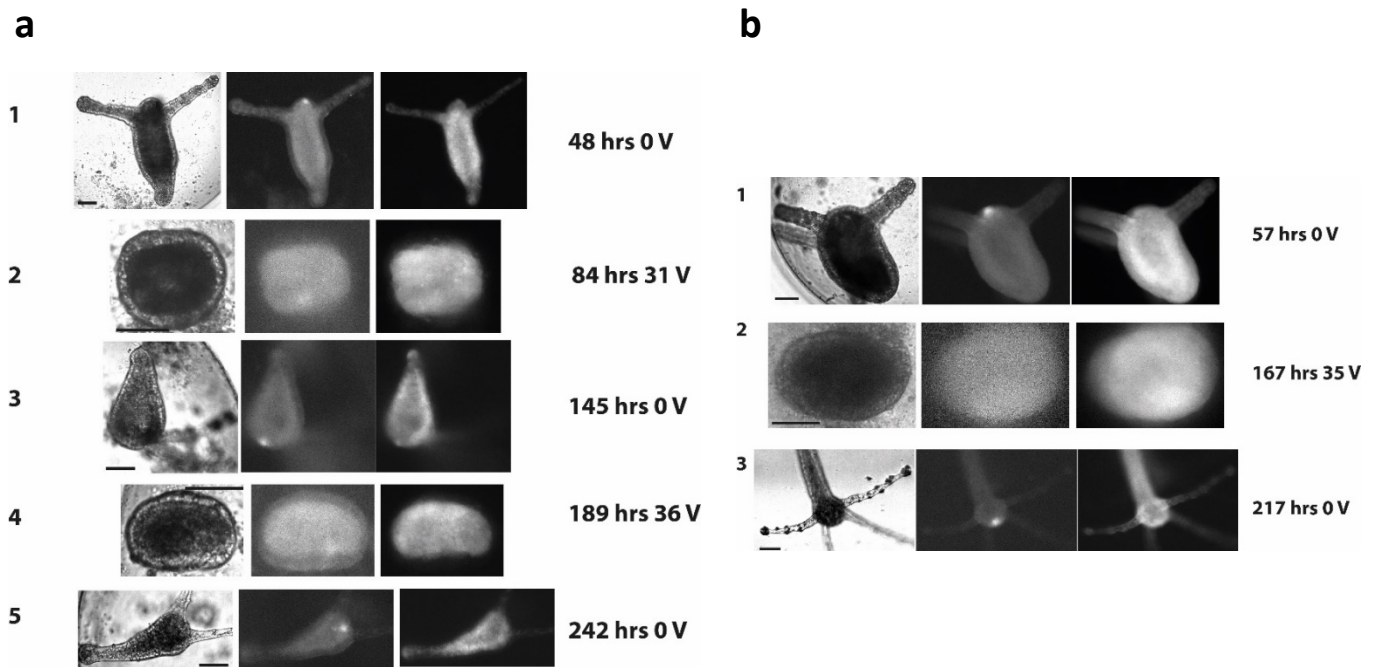


Fig. S3: Examples of the *Wnt3* activity decay upon reversal of morphogenesis. Transgenic *Hydra* expressing a GFP probe under the control of the *Wnt3* promoter is imaged under a fluorescence microscope with time-lapse images taken every 1 min (as in Fig. 2 in the main text). This transgenic *Hydra* is also expressing dsRED (RFP) under the control of the ubiquitous actin promoter, serving as a fluorescence reference. Two experiments (a, b) are shown as a sequence of 3 images (from left: bright field, GFP, RFP) over time. The running time (hrs from the point of tissue excision) and the applied external voltage are depicted to the right of the images. A clear fluorescence signal of GFP under the *Wnt3* promoter at the head of a transgenic *Hydra* emerges after the initial spheroid tissue regenerates (1) and decays upon the reversal of morphogenesis in (2). The *Wnt3*-activated fluorescence reemerges upon renewal regeneration after the voltage is switched off in (3). The experiment in (a) demonstrates a second cycle of reversal morphogenesis (4) and renewal of regeneration leading to re-emergence of the *Wnt3*-activity fluorescence signal. Bars 100 μ m scale.

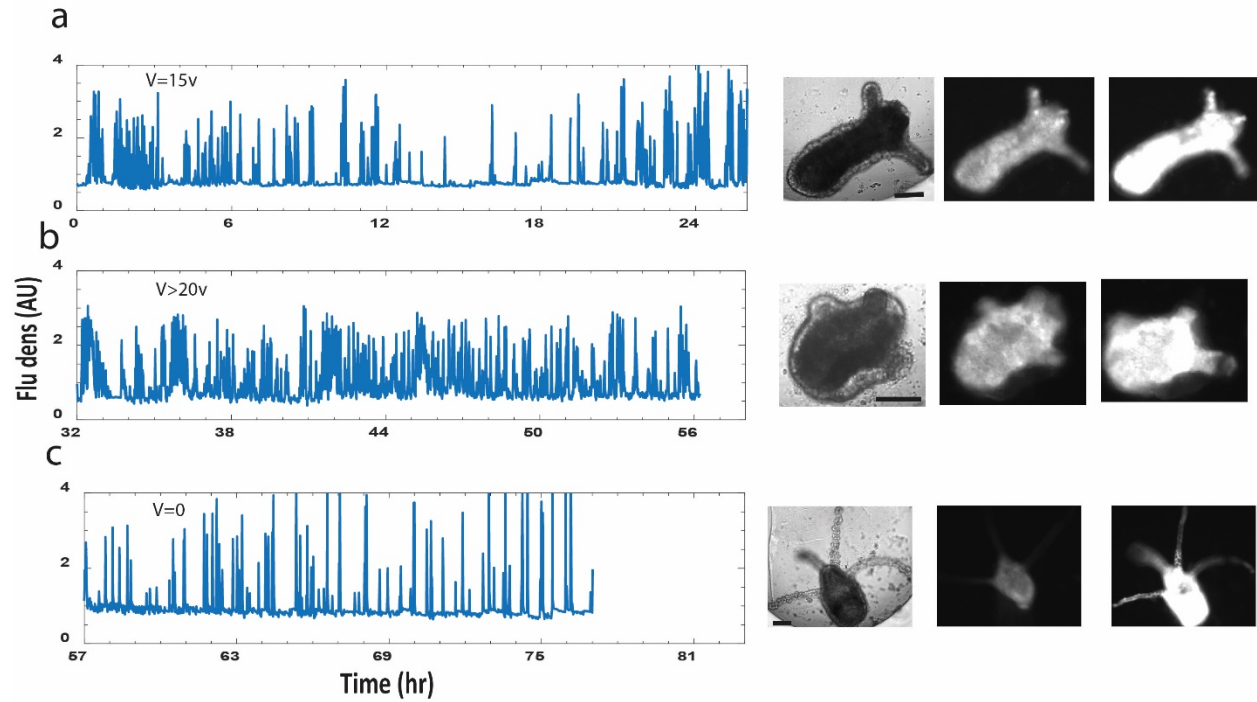


Fig. S4: Calcium dynamics. (a) Ca^{2+} dynamics as measured by the fluorescence density (fluorescence signal per unit area) as in Fig. 3c in the main text. The measurement starts 3 hrs after the tissue excision at 15 V which is below the critical value (a). The voltage is then increased to higher values (24 V) in (b) and then switched off in (c). The images on the right show microscopy images of the sample at the end point of each trace (from left: bright field, low and high Ca^{2+} activity depicted by the fluorescence images). Bars 100 μm scale.

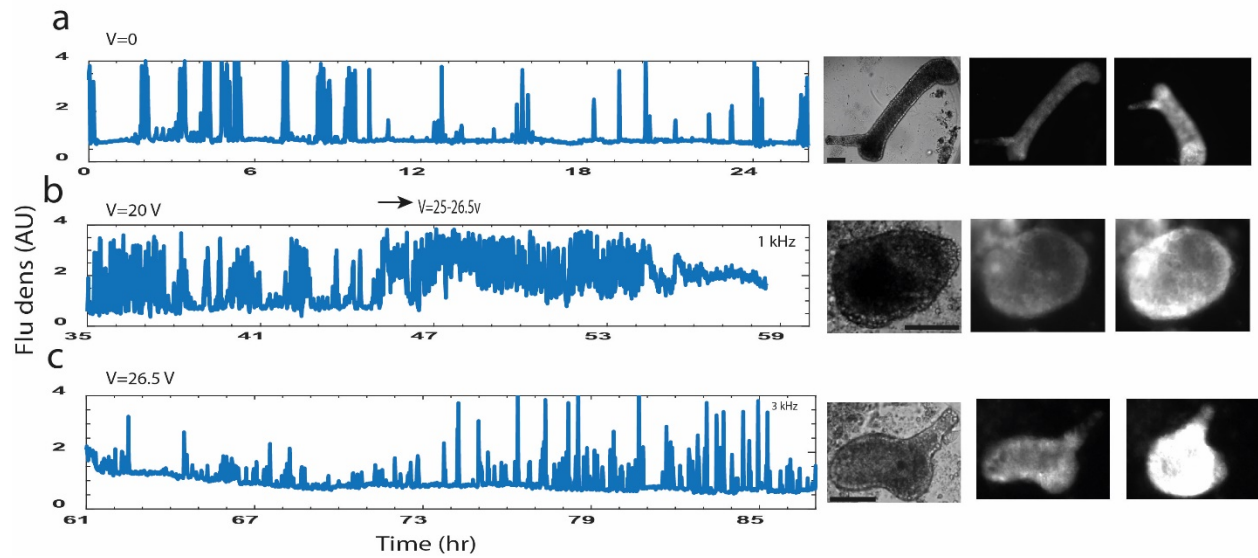


Fig. S5: Frequency cutoff. Ca^{2+} activity measured by the fluorescence density as in Fig. 4a in the main text, for two different frequencies of the external electric field. The measurement starts 3 hrs after the tissue excision at $V=0$ (a) and continues at high voltage (20-26.5 V) at 1 kHz (b), showing enhanced Ca^{2+} activity. Switching the frequency of the external AC field to 3 kHz, while maintaining the voltage amplitude at 26.5 V, shows reduction in Ca^{2+} activity (c). The images at the right show microscopy images of the sample at the end point of each trace (from left: bright field, low and high Ca^{2+} activity depicted by the fluorescence images). They show that the tissue fully regenerates for $V=0$ and then folds back into a spheroid morphology at high voltage, while resumption of a fully regenerated *Hydra* is observed upon the switch of the frequency to 3 kHz. Bars 100 μm scale.

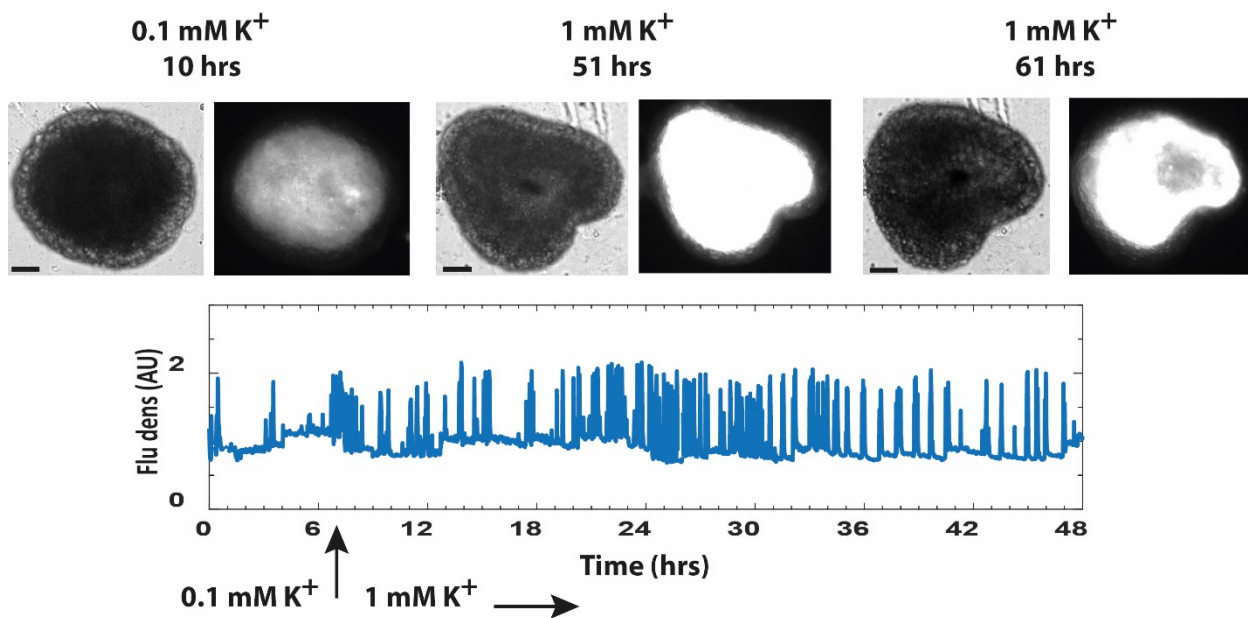


Fig. S6: Stimulation by elevated potassium. The trace shows enhanced Ca^{2+} activity measured by fluorescence density upon the increase of the potassium (K^+) in the medium from 0.1 mM (normal medium) to 1 mM at the time marked by the arrow. The measurement starts 3 hrs after the tissue excision. Microscopy images of the sample at the indicated time points (hrs from the excision point) and K^+ concentrations are shown above the trace in pairs (left: bright field; right Ca^{2+} activity depicted by the fluorescence images). The images show that after 61 hrs there are no signs of regeneration in 1 mM K^+ while all samples at the normal *Hydra* medium (0.1 mM K^+) regenerate within 55 hrs.

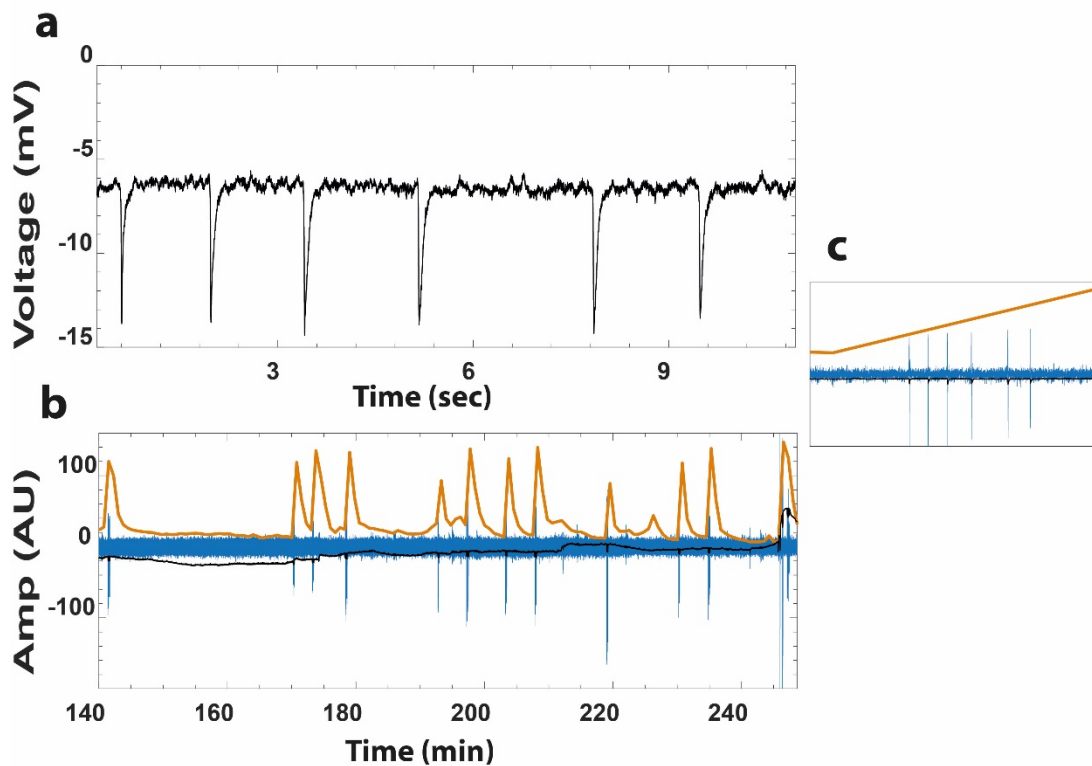


Fig. S7a: Electrical measurement in a tissue fragment. (a) Voltage measurement of a spike burst by a silver-chloride electrode inserted into a tissue fragment embedded in a low-melting 2% agarose gel. (b) Simultaneous recording of Ca²⁺ activity by fluorescence microscopy (yellow) and the voltage by an electrode (black). The blue trace shows the voltage spikes extracted from the original voltage measurement by subtracting a smoothed trace (0.1 sec window) from the original one and amplifying the resulting trace (distorting the uniphase spikes, but allowing easy identification of them). Each Ca²⁺ spike follows a burst of electrical spikes. The burst in (a) is a zoom over a burst near 190 min in (b). (c) Zoom over one of the Ca²⁺ spike events in (b), showing clearly the burst of electrical spikes.

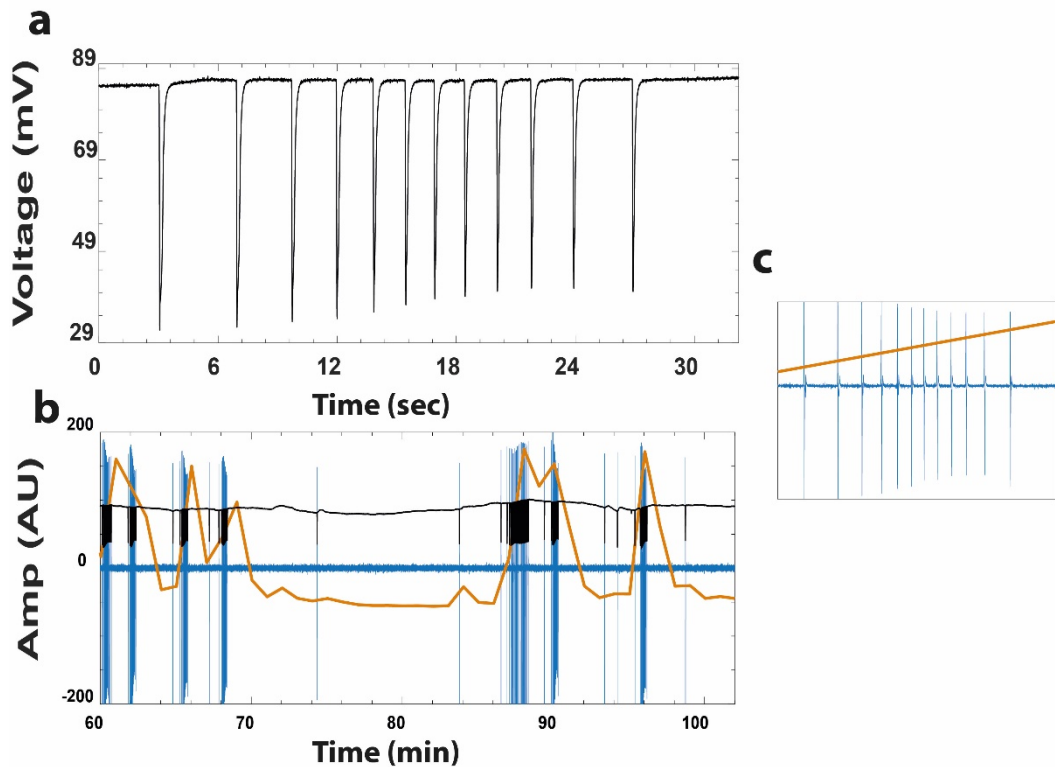


Fig. S7b: Electrical measurement in a spheroid. (a) Voltage measurement of a spike burst by a silver-chloride electrode inserted into a tissue spheroid (around 3 hrs after excision and folding in solution) embedded in a low-melting 2% agarose gel. (b) The simultaneously recording of Ca^{2+} activity by fluorescence microscopy (yellow) and the voltage by an electrode (black). The blue trace shows the voltage spikes extracted from the original voltage measurement as in Fig. S7a. Each Ca^{2+} spike follows a burst of electrical spikes. The burst in (a) is a zoom over a burst near 65 min in (b). (c) Zoom over one of the Ca^{2+} spike events in (b), showing clearly the burst of electrical spikes.

Supplementary Videos:

Movie S1: Reversal of morphogenesis. Bright-field microscopy movie of a tissue spheroid regenerating into a mature *Hydra* and then folding back its morphology under an electric field. The reversed tissue regenerates again upon the reduction of the external voltage to zero. A second round of reversal of morphogenesis then follows. Note the differences in the critical voltages required for reversal of morphogenesis for the first and second rounds; the voltage range in the first round is 20-30 V while in the second round is 30-40 V. The scale of the image is ~ 1.1 mm and the running time is from the point of tissue excision.

Movie S2: Decay of *Wnt3* during reversal of morphogenesis. The same sample as in Movie S1 is observed under a fluorescence microscope for GFP (left) and RFP (right). The GFP is under the *Wnt3* promoter and the RFP is under the control of the ubiquitous *Hydra* actin promoter and serves as a fluorescence reference. The movie shows the two rounds of reversal of morphogenesis as in Movie 1. The scale of the image is ~ 1.1 mm and the running time is from the point of tissue excision.

Movie S3: Dynamics of Ca^{2+} in reversal of morphogenesis under an electric field. Fluorescence microscopy time-lapse of a strain expressing the GCaMP6s probe reporting Ca^{2+} activity in the epithelial cells. The tissue spheroid regenerates under a voltage below the critical value and then folds back as the voltage is increased. The tissue regenerates again upon switching the voltage to zero. The scale of the image is ~ 1.1 mm and the running time is from the point of tissue excision.

Movie S4: Frequency threshold of the external field. Bright-field microscopy of a tissue under an external AC electric field at two different frequencies. At 1 kHz and voltage above criticality, the *Hydra* exhibits reversal of morphogenesis and folds into a spheroid while it regenerates again at 3 kHz under the same voltage. The movie shows two rounds of the backward-forward morphogenesis cycle under the frequency switch. The scale of the image is ~ 1.1 mm and the running time is from the point of tissue excision.